

Remarkable Stability of Small Cobalt Nanoparticles Prepared by Sodium Borohydride Reduction in the Fischer-Tropsch Synthesis

Jorge A. Delgado,^a Carmen Claver,^{a,b} Sergio Castellón,^c Daniel Curulla-Ferré,^d Vitaly V. Ordomsky,^e and Cyril Godard^{b*}

^a Centre Tecnològic de la Química, 43007, Tarragona, Spain.

^b Departament de Química Física i Inorgànica, Universitat Rovira I Virgili, C/ Marcel·li Domingo s/n, 43007 Tarragona, Spain. Fax: (+34) 977 559563; E-mail: cyril.godard@urv.cat

^c Departament de Química Analítica i Orgànica, Universitat Rovira i Virgili, C/ Marcel·li Domingo s/n, 43007 Tarragona, Spain

^d Total Research and Technology Feluy, Zone Industrielle Feluy C, B-7181 Seneffe, Belgium

^e Unité de Catalyse et de Chimie du Solide, USTL-ENSCL-EC Lille, Bât. C3, Cite Scientifique, 59655 Villeneuve d'Ascq, France. Fax: (+33) 320 436 561.

Abstract

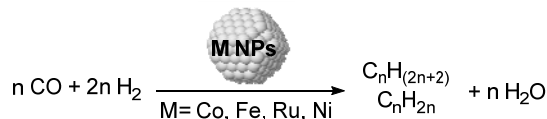
Cobalt nanoparticles in the range of 1.7-7 nm were synthesized in water using sodium borohydride as reducing agent and subsequently immobilized on TiO₂. Both colloidal and TiO₂ supported NPs were characterized by TEM, XRD, HRTEM, XPS, TGA, ICP techniques and their catalytic performance of the supported catalysts evaluated in the Fischer-Tropsch synthesis. As a general trend, an increase in activity and TOF was observed when the particle size decreased. These results were rationalized by the higher reducibility of the catalysts bearing the smaller nanoparticles. The unconventional stability of these relatively small CoNPs in FTS was attributed to the promoting effect of boron on the stability of the cobalt nanocrystals.

Keywords: Fischer-Tropsch synthesis, cobalt nanoparticles, sodium borohydride, titanium oxide, boron promotion.

1 Introduction

The increasing worldwide energy demand has made major companies to consider alternative feedstocks such as natural gas, coal and biomass to replace fossil fuels.[1] In this context, the Fischer-Tropsch Synthesis (FTS) has been considered a key process of the biomass-to-liquids (BTL), gas-to-liquids (GTL) and solid-to-liquids technologies (STL)[2] since through this catalytic reaction, syngas can be transformed into high quality synthetic fuels (Scheme

1).[3-5] FTS is catalyzed by several transition metals including Ru, Co and Fe. However, cobalt based catalysts are more attractive from an industrial point of view due to their higher hydrocarbon productivity, good stability and commercial availability.[1]



Scheme 1. Fischer-Tropsch synthesis catalyzed by metal nanoparticles

The performance of supported catalysts is largely influenced not only by the properties of the support and the derived metal/support interactions,[6] but also by the method of preparation of the catalysts.[7] Among the methods reported for cobalt based catalysts, the most widely used are impregnation,[8, 9] deposition-precipitation,[10, 11] and the colloidal-immobilization method.[12-15] For incipient wetness impregnation methodology, the formation of hardly reducible metal-support mixed compounds during the calcination processes is often a drawback. In contrast, the immobilization of previously formed colloidal metal nanoparticles exhibits the advantage of the soft heterogenization of well-defined active phases, maintaining the characteristics of the colloidal nanomaterial. In addition, colloidal synthesis has been widely used as an efficient route to control metal particle size, and structure of metal NPs.[16] The use of colloidal methods has been reported for the preparation of ruthenium[17-23] and cobalt catalysts[24-31] for FTS.

One of the simplest procedures for the synthesis of metal nanoparticles consists in the chemical reduction of metal salts in water using NaBH₄ as reducing agent. Metal nanoparticles obtained from this approach are often small, being ideal when the catalyst productivity is boosted by the increase of the surface area of the active metal. For the case of the Fischer-Tropsch synthesis, the effect of the cobalt particle size at the lower limit of the nanoscale has been always a motif of discussion. Although many of these studies pointed that cobalt nanoparticles (CoNPs) below 10-6 nm resulted in less active catalysts compared to cobalt particles of larger sizes,[32-36] there are some reports showing the opposite trend.[12, 37, 38]

Over the last decade, several groups have reported the preparation of colloidal cobalt nanoparticles and their application in the Fischer-Tropsch Synthesis.[25, 29, 39] Dupont and co-workers reported the preparation of CoNPs by decomposition of organometallic precursors using ionic liquids as solvent and stabilizing agents.[29-31] Very recently, our group reported the effect of the pH[39] and of the addition of organic co-solvents in the Aqueous phase Fischer-Tropsch Synthesis (AFTS) catalyzed by PVP stabilized colloidal CoNPs.[40] It was concluded that the product selectivity strongly depends on the pH and composition of the

solvent used in catalysis. Kou and co-workers have also reported the application of colloidal cobalt nanoparticles stabilized by PVP as catalysts of the AFTS.[24, 25, 27, 28]. These authors tested CoNPs reduced by LiBEt_3H and NaBH_4 in the AFTS, and proposed that B-doping could affect negatively the catalytic performance of these NPs, however, no details on the nanoparticle structure or cobalt-boron interaction were given.[25] In contrast, Saeys and co-workers reported that the addition of boron exerts a positive effect in terms of stability of cobalt supported catalysts in the FTS.[41] This conclusion was supported on DFT calculations which suggested that boron promotion can selectively block the deposition, nucleation, and growth of resilient carbon species responsible of catalyst deactivation. This concept was experimentally verified on a 20 wt.% $\text{Co}/\text{Al}_2\text{O}_3$ catalyst promoted by 0.5 wt.% boron and comprised by CoNPs of *ca.* 10 nm, however no reports on such an effect for smaller cobalt particles has been reported to date.

In the present work, the synthesis of well defined CoNPs in the range of 1.6-7 nm by chemical reduction using sodium borohydride and their subsequent immobilisation onto TiO_2 are described. This synthetic approach allowed the fine modulation of the cobalt particle size and the easy immobilization in the solid support, thus avoiding intermediate calcination treatments which often results in undesirable cobalt-support reactions. The structure and composition of these cobalt nanoparticles and the corresponding supported catalysts were investigated and their catalytic performance evaluated in FTS. The catalytic experiments provided insights on the promoting effect of boron on the stability of very small CoNPs in FTS.

2 Experimental

2.1. Materials and methods

All syntheses of CoNPs were carried under aerobic conditions using a mechanical stirrer. Milli-Q water was used for all the experiments. Solvents were purchased from Merck and used as received. $\text{CoCl}_2 \cdot 6\text{H}_2\text{O}$, NaBH_4 and PVP K-30 and were purchased from Sigma-Aldrich. Hydrogen (5.0) was purchased from Air Liquide and CO (4.7) and argon (5.0) from Carbueros Metálicos.

Transmission electron microscopy (TEM) and high resolution transmission electron microscopy (HR-TEM) measurements were performed using a Zeiss 10 CA and a JEOL 2011(FEG) electron microscopes respectively. X-ray diffraction (XRD) patterns were recorded on a Siemens D5000 diffractometer using $\text{Cu K}\alpha$ radiation. Continuous scan mode was used to collect data over the 2θ range of 15° to 90° . X-ray Photoelectron Spectroscopy (XPS) data were obtained with a PHI 5500 Multitechnique System electron spectrometer from Physical Electronics using 350 W $\text{Al K}\alpha$ radiation. The base pressure was about 2×10^{-8} torr. Fourier transform infrared (FT-IR) spectra were obtained as potassium bromide pellets with a resolution of 4 cm^{-1} and 32 scans in the range of $400\text{--}4000 \text{ cm}^{-1}$ using a Bruker Equinox 55

spectrophotometer. Thermogravimetric analysis (TGA) were obtained on a Mettler TGA/SDTA851e thermobalance. Samples (*ca.* 0.01 g) were heated from room temperature up to 900 °C with 10 K min⁻¹ under nitrogen flow using alumina holders. Elemental analysis of cobalt were performed by inductively coupled plasma-optical emission spectrometry (ICP-OES) using a Spectro Arcos FHS-16 spectrometer. Temperature programmed reduction under H₂ (TPR) was carried out using a ChemBET™ TPR/TPD (Quantachrome). The samples (*ca.* 0.1 g) were heated up to 900 °C under 5% H₂/Ar flow (30 cm³ min⁻¹) using alumina crisols. The rate of temperature ramp was 10 °C min⁻¹. BET areas were calculated from the nitrogen adsorption isotherms at -196 °C using a Quadrasorb SI equipment. All the samples were degased at 90 °C during 24 h prior to the physisorption measurements.

2.2. Synthesis of colloidal cobalt nanoparticles (Co1-4)

CoNPs were synthesized by chemical reduction of cobalt dichloride in the presence of polyvinylpyrrolidone (PVP) as stabilizer and using sodium borohydride as reducing agent. The size of the **Co1-4** was modulated through the variation of the concentration of reagents. As a standard procedure, 0.226g of CoCl₂.6H₂O (0.931 mmol) was dissolved in H₂O containing the polymer stabilizant (2.066 g of PVP-K30). The volume of water used to dissolve both PVP and the cobalt salt was 12.5, 50, 200 and 800 ml for **Co1-4** respectively. Then, a freshly prepared solution of 0.358 g of NaBH₄ (9.31 mmol) in H₂O was added at room temperature during at a rate of 3 ml/min. The volume of water used to dissolve the NaBH₄ was 4.1, 16.6, 66 and 264 ml for **Co1-4** respectively. The solution was maintained with a vigorous mechanical stirring for 2 h. Then 100 µl of the colloidal solution was centrifuged, washed with water and re-dispersed by sonication. Three drops of the obtained colloidal solution was deposited on a Cu-formvar or holey carbon grids for TEM or HR-TEM analysis. For the isolation of the CoNPs, the freshly prepared NPs were initially precipitated by a strong magnetic field and the supernatant was decanted. Then, the precipitated NPs were rinsed with water to remove the excess of salts and PVP. The decantation and washing process was repeated three times with water, then with ethanol and hexane. The resulted CoNPs were finally dried under vacuum and kept in the glove box. The size, the crystalline structure and oxidation state of the CoNPs were studied using transmission electron microscopy (TEM), HR-TEM, X-ray diffraction (XRD), and X-ray photoelectron spectroscopy (XPS) respectively. The composition of the CoNPs was studied using FTIR, TGA and ICP-OES.

2.3. Immobilization of cobalt nanoparticles on TiO₂ (Co1-4/TiO₂)

Isolated CoNPs (55 mg approximately) were re-suspended in 20ml of hexane and sonicated during 3 minutes. Separately, a suspension of TiO₂ (0.490 g of 20 nm nanopowder, Degussa P25, 35-65 m²/g) in 40 ml of hexane was firstly sonicated during 1 min and then

mechanically stirred. The amount of TiO₂ was the corresponding to obtain a 10wt% Co catalyst. Then the suspension of CoNPs in hexane was added dropwise over the stirred suspension of TiO₂ and the resultant stirred during 30min more. The gray suspension was then sonicated during 3 min to disperse well the CoNPs on the support and the resultant solid was magnetically precipitated, the hexane removed and the solid dried under vacuum.

Since the obtained powders were too fine to be suitable for the microreactors, they were pelletized using a press then crushed and sieved to get grain sizes between the 0.300 - 0.150 mm. The obtained materials were then used for the catalytic test.

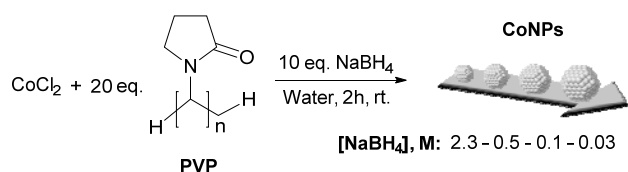
2.4. Fischer-Tropsch catalytic experiments using the TiO₂ supported catalysts (Co1-4/TiO₂)

Fischer-Tropsch experiments using supported catalysts were carried out in fixed bed reactor ($d_{\text{int}} = 2$ mm) operating at a total pressure of 20 bar, H₂/CO = 2 molar ratio and GHSV = 6700 cm³/g h. The catalyst loading in the was 100 mg. Prior to the catalytic test, all the samples were activated in a flow of pure hydrogen at atmospheric pressure during 10 h at 673 K with at GHSV = 2 NL h⁻¹ g⁻¹. During the reduction, the temperature ramp was 1 K/min. After the activation, the catalysts were cooled down to 433 K and a flow of premixed syngas was gradually introduced through the catalysts. When pressure attained 20 bar, the temperature was slowly increased to 513 K with a ramp of 1 K/min. Gaseous reaction products were analyzed on-line by gas chromatography. Catalytic rates and selectivities were measured at the steady-state regime after 46 h time-on-stream. The reaction rates expressed in cobalt time yield h⁻¹, are defined as the moles of CO converted per mol of Co per hour. The product selectivity (*S*) is reported as the wt% of a given product.

3. Results and Discussion

3.1. Synthesis and characterization of CoNPs

The cobalt nanoparticles synthesized in this work were prepared by chemical reduction of CoCl₂ in water using NaBH₄ as reducing agent and PVP as stabilizer (Scheme 2). The TEM micrographs and size histograms of **Co1-4** are displayed in Figure 1. According to TEM analysis, spherical cobalt nanoparticles of diameters between 1.7 to 7.0 nm were obtained. As a general trend, it was observed that increasing the concentrations of both NaBH₄ and CoCl₂/PVP solutions, resulted in a decrease of the CoNPs size.



Scheme 2. Synthesis of the CoNPs with variation of the NaBH₄ concentration.

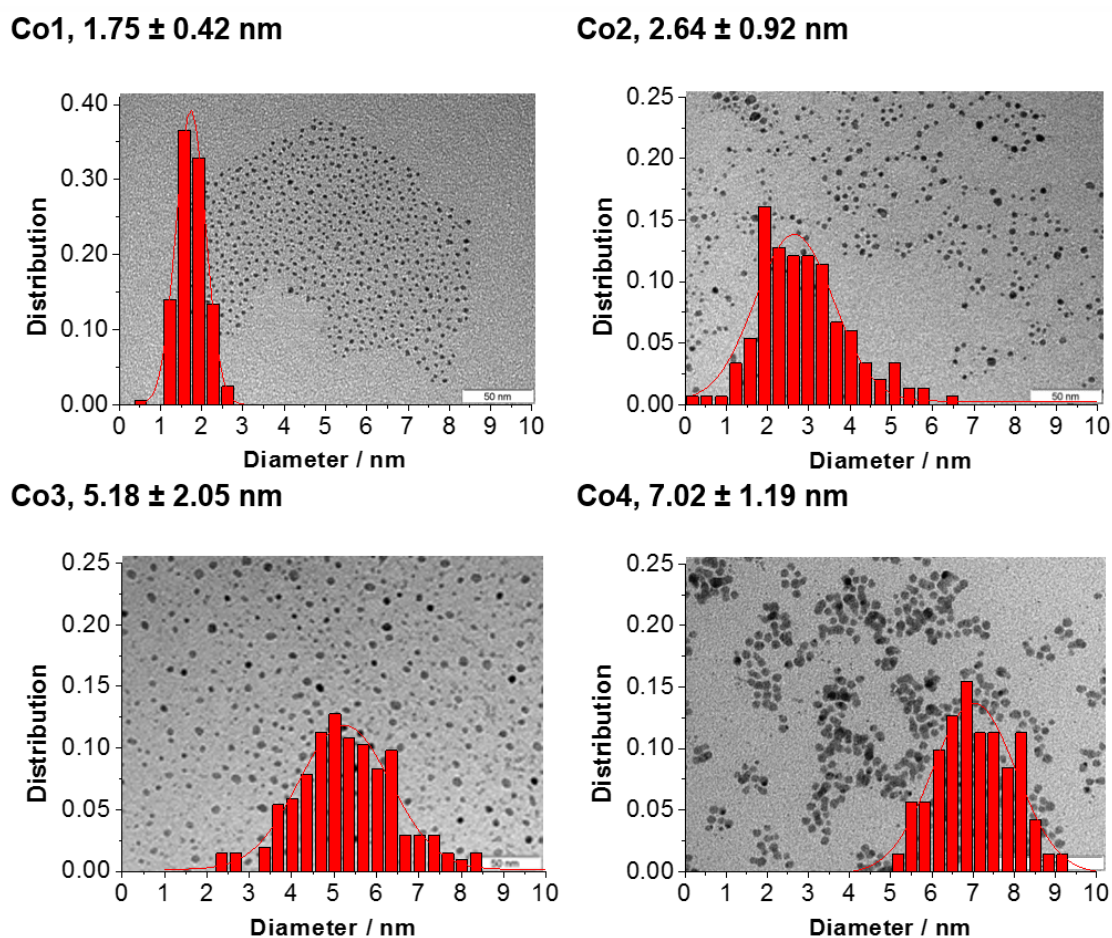


Figure 1. TEM micrographs and size histograms of **Co1-4**.

The formation of smaller particles under high NaBH₄ concentrations is explained by the higher nucleation rate, which is the responsible of the formation of a large number of cobalt seeds, in comparison with the growth rate. A similar relationship between the concentration of NaBH₄ with the cobalt particle size was reported by Wang *et al* for the preparation of CoNPs supported in faujasite zeolites.[42]

The size and the fine structure of **Co2** were studied by High-Resolution Transmission Electron Microscopy (Supporting Information). With this technique, particles of 2.6 nm were observed, in agreement with previous TEM analysis (2.64 ± 0.92 nm). The diffuse rings appreciated in the electron diffraction pattern suggested an amorphous structure for the nanoparticles.

The XRD pattern of the series of CoNPs (Figure 2), exhibited a broad band centred at 45°, which became sharper when the particle size increased from 1.6 to 7.0 nm (**Co1-Co4**). In

addition, two signals of low intensity at 34 and 60° were appreciated in **Co3** and **Co4**. However, none of them could be unambiguously attributed to cobalt phases. The broadening of XRD lines is frequently related to the decrease of the crystallite size but also to the presence of strained and imperfect crystals. Similar XRD patterns have been reported in the literature for CoNPs synthesized by chemical reduction using NaBH₄ as reducing agent.[43, 44]

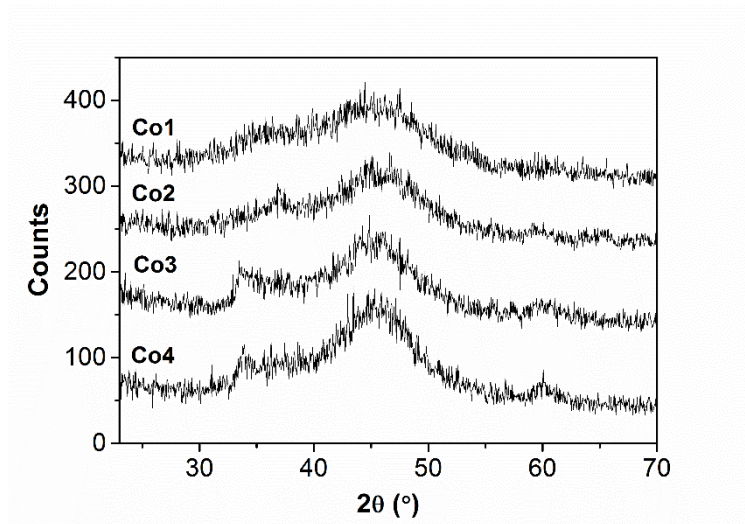


Figure 2. XRD patterns of **Co1-4** NPs.

In order to gain insights into the structure of the nanoparticles, samples of **Co1-4** were subjected to a thermal treatment following the method described by Glavee *et al*, with the aim to force the crystallization/sintering of the NPs.[45] For this purpose, the nanoparticles were heated at 500 °C within 2-5 min under argon flow and kept at this temperature for 2 h. The diffraction pattern of the thermally treated samples exhibited fcc and hcp cobalt crystalline phases (Figure 3) together with a defined signal of B(OH)₃ located at 28°. Curiously, **Co1** exhibited additional peaks corresponding to Co₂B-bct, which did not appear in the other samples. It was therefore concluded that **Co1-4** are constituted by a mixture of cobalt, Co₂B and B(OH)₃ phases.

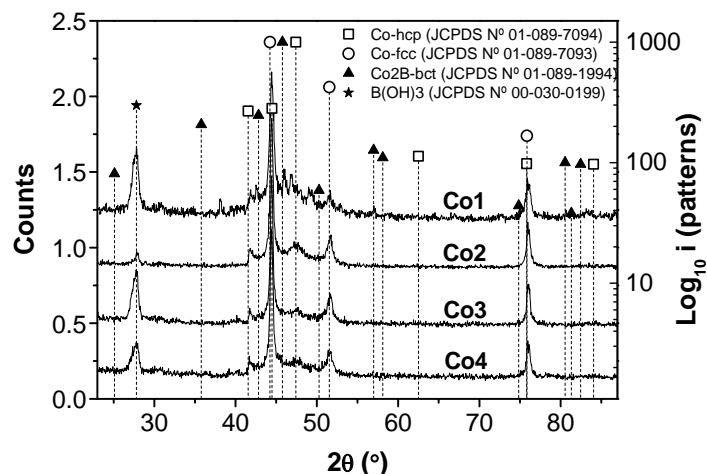


Figure 3. XRD patterns of **Co1-4** treated at 500 °C for 2h under argon.

Surface analysis of the CoNPs synthesised in this study was also performed by X-ray photoelectron spectroscopy (XPS). The full XPS spectra of **Co1-4** revealed the presence of Na, Co, O, N, C and B, according to the peaks observed at their characteristic binding energies (1071.6; 781.5; 530.9; 399.2; 284.5 and 191.1 eV respectively). Deconvolution of the Co 2p_{3/2} spin orbit peaks revealed that the reduction degree at the nanoparticle surface decreases from 38 to 12% in the series **Co1-4**, according to the increase of the particle size from 1.7 to 7 nm.

Quantification of the cobalt and boron content in **Co1-4** performed by ICP revealed that the Co/B atom ratio was in the range 2.1-2.8 for the series of NPs (*ca.* 10 wt. % of boron). Curiously, Kou and co-workers reported Co/B values of *ca.* 0.2 for CoNPs of 14 ± 6 nm synthesized under similar conditions.[25] Such low values suggest a considerably higher boron content than those measured in **Co1-4**, which can be attributed to the anaerobic conditions used by Kou for the synthesis of the CoNPs, according to Glavee,[45]. In the present work no clear trend between the content of boron and the particle size of the CoNPs was observed.

The presence of PVP and the thermal stability of **Co1-4** were examined by thermogravimetric analysis. The thermograms of **Co1-4** exhibited a first weight loss in the range of 90-110 °C (-5 wt% aprox.) which was attributed to the loss of adsorbed solvent. However, no appreciable weight loss was observed at the decomposition temperature of PVP (430 °C). Additionally, no characteristic signals of PVP were detected by FTIR in the CoNPs. It was therefore concluded that there is no remaining PVP at the surface of **Co1-4** after the workup.

To summarize, CoNPs of sizes between 1.7 to 7.0 nm were synthesized by reduction of CoCl₂ using NaBH₄ in water. Structural analysis by HR-TEM and XRD indicated the amorphous structure of the NPs and revealed the presence of metallic cobalt, Co₂B and B(OH)₃ phases. Surface analysis by XPS indicated that the smaller the cobalt particle, the higher the

reduction degree of the nanoparticle is. Finally, analysis by FTIR and TGA demonstrated the absence of PVP at the surface of these NPs after work-up.

3.2. Characterization of TiO₂ supported catalysts (Co1-4/TiO₂)

Supported Co/TiO₂ catalysts were prepared by impregnation of the colloidal CoNPs, via the mixing of the CoNPs and TiO₂ nanopowder suspensions in hexane. TEM analysis showed that the particle size of the CoNPs was maintained after immobilization on TiO₂ (Figure 4).

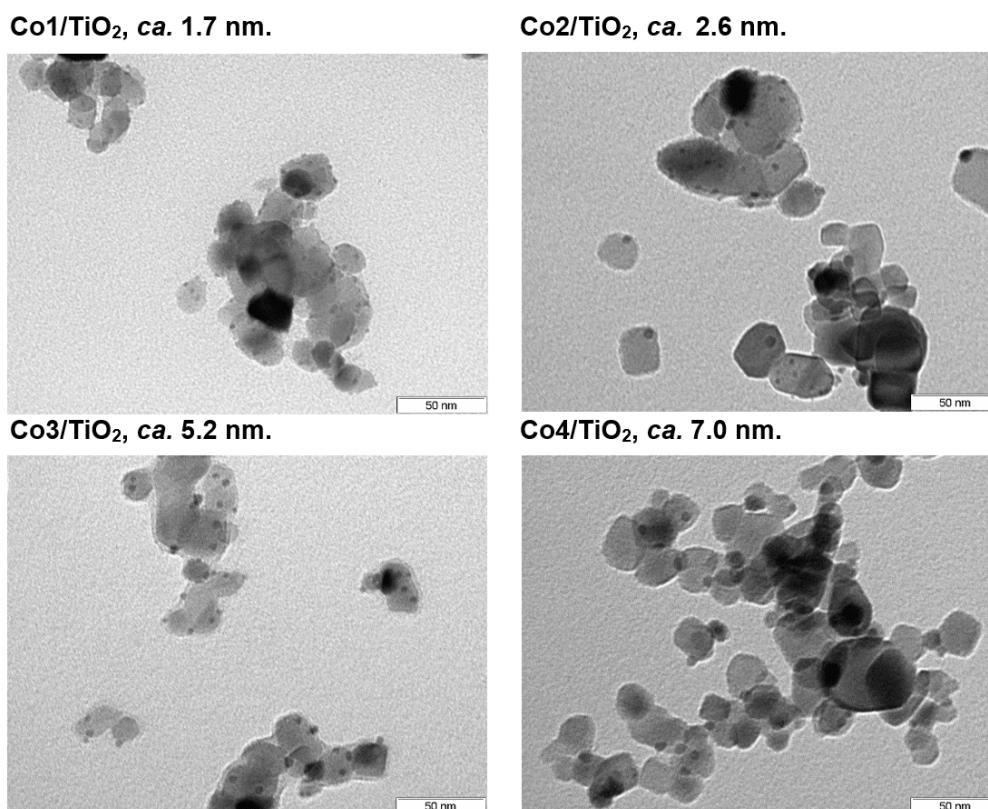


Figure 4. TEM micrographs of Co1-4/TiO₂ supported catalysts.

The HR-TEM micrograph of Co2/TiO₂ displayed in Figure 5, showed that CoNPs are situated at the borders of a TiO₂ crystal (indicated by arrows). The fine structure of the support is appreciated and the electron diffraction of the dotted area present characteristic signals of anatase planes (hkl: 101 and 004, Sys: Tetragonal, S.G: I4₁/amd).

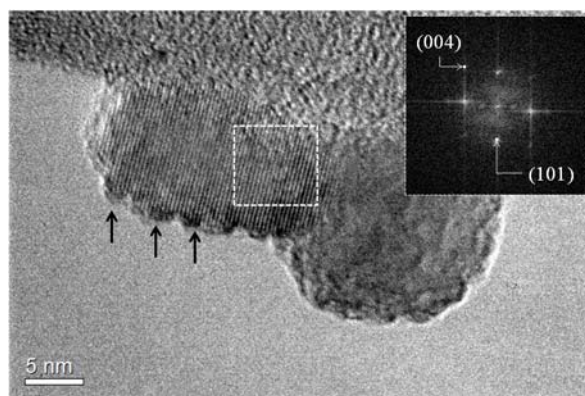


Figure 5. HR-TEM micrograph and electron diffraction of **Co2/TiO₂**.

Structural analysis of the supported catalysts was also performed by XRD (Supporting Information). Despite that the anatase crystalline phase predominated over the rutile phase (85 vs. 15%), the main signal of the CoNPs at 45° was overlapped with a signal of the rutile phase.

Surface analysis of the supported catalysts was also performed by XPS and deconvolution of the Co 2p_{3/2} spin orbit peaks confirmed that the reduction degree at the metal surface increased for smaller nanoparticles.

The reducibility of the supported catalysts **Co1-4/TiO₂** was analyzed by temperature programmed reduction (TPR). Due to the partial reduction of the CoNPs (intrinsic of the reduction methodology used), low signals were observed during the analysis of the fresh catalysts (Supporting Information). For this reason, with the aim to increase the H₂ consumption, a soft passivation process was performed for all the catalysts prior to TPR analysis (100 °C, 30 min under air).

As displayed in Figure 6, at least two reduction bands were observed from their TPR profile at *ca.* 300-450 and 450-600 °C. The peak at 300–400 °C corresponds to the reduction of Co₃O₄ to CoO and that at 400–600 °C to the reduction of CoO to Co metal.[7] The TPR spectra of **Co1/TiO₂** corresponding to the NPs of 1.7 nm, displayed bands shifted to lower temperatures when compared to the catalyst containing the largest cobalt NPs, 7.0 nm (**Co4/TiO₂**).

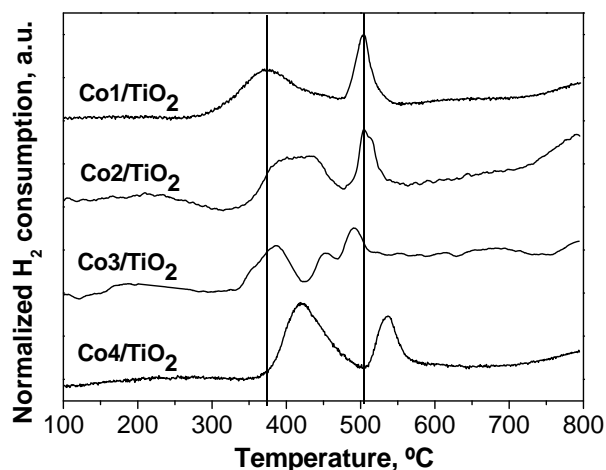


Figure 6. H₂-TPR profiles of **Co1-4/TiO₂** catalysts.

Nitrogen physisorption analyses were also realized on supported catalysts. The BET areas of the series of catalysts **Co1-4/TiO₂** ranged between 44 and 62 m²/g, values which are slightly larger than that measured for TiO₂ alone (43 m²/g). ICP analysis of the supported catalysts revealed that the cobalt loading for the series ranged between 7-10 wt %.

To summarize, the supported catalysts **Co1-4/TiO₂** were prepared by impregnation of the corresponding colloidal NPs **Co1-4** on TiO₂. Analysis of the supported catalysts by TEM and XPS confirmed the particle sizes and the trend in reduction degree determined in the colloidal NPs. Finally, analysis of **Co1-4/TiO₂** by TPR revealed that the reducibility of the catalysts increased with the decrease of the cobalt particle size.

3.3. Fischer-Tropsch synthesis using TiO₂ supported CoNPs (**Co1-4/TiO₂**)

Fischer-Tropsch catalytic experiments were performed using the TiO₂ supported catalysts **Co1-4/TiO₂** in micro fixed bed reactors. Since the catalysts had not exactly the same cobalt content and because of the differences in the particle size of the CoNPs, surface specific activity (cobalt site yield = mol of CO converted per mol of surface Co, per unit of time) were used instead of CO conversions to represent the catalytic activity. The cobalt site yields and product selectivity obtained at 240 °C after 46 h of reaction are displayed in Table 1. Comparing the series of catalysts (Table 1, entry 1-4), it is clearly observed that increasing the cobalt particle size (**Co1/TiO₂** to **Co4/TiO₂**) resulted in the progressive decrease of the cobalt site yield from 18.5 to 2.1 h⁻¹.

Table 1. Fischer-Tropsch synthesis in fixed bed reactor catalyzed by TiO₂ supported CoNPs (**Co1-**

4/TiO₂)^a

E.	Catalyst	Co size, nm	Cobalt site yield, h ^{-1,b}	Selectivity, Wt%					α
				CO ₂	CH ₄	C ₂₋₄	C ₅₋₁₂	C ₁₂₊	
1	Co1/TiO₂	1.75	18.5	0.3	12.1	16.5	19.8	51.3	0.71
2	Co2/TiO₂	2.64	12.7	0	10.5	17.4	19.0	53.0	0.76
3	Co3/TiO₂	5.18	6.6	0	17.4	23.6	27.0	32.1	*
4	Co4/TiO₂	7.02	2.1	*	*	*	*	*	0.87

^a Conditions: Catalyst loading=8-12wt%, 20 bar H₂/CO/N₂ (2:1:0.15), 5.62 ml/min, 240 °C, CO conversions at 46 h; ^b cobalt site yield = mol of CO converted per mol of surface Co, per unit of time. * Not available information.

It should be noted that due to the low activity of **Co4/TiO₂**, the obtained products were hardly quantified. The CO₂ and CH₄ selectivity for the series of catalysts were below 0.4 % and in the range of 10-17% respectively. The C₂₋₄ selectivity was observed to increase from 16.5 to 23.6% for the catalysts **Co1-3/TiO₂** in which the cobalt particle size increased from 1.7 to 5.2 nm. Concerning the chain growth probability, the alpha values increased from 0.71 to 0.87 when the particle size of the CoNPs increased (**Co1-4/TiO₂**) according to the ASF distributions displayed in Figure 7.

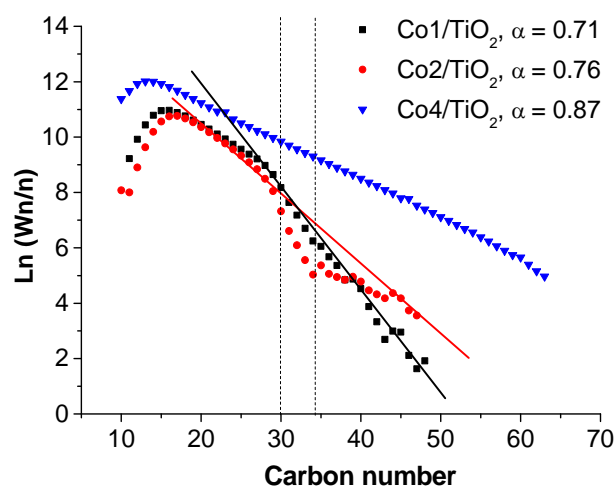


Figure 7. ASF distributions of **Co1-4/TiO₂**.

It is noteworthy that the catalyst bearing the smallest CoNPs, **Co1/TiO₂** and **Co2/TiO₂** (1.7 and 2.6 nm) exhibited an inflexion in the distribution near C₃₀ and hydrocarbons longer than C₅₀ were not detected. In contrast, the catalysts with the largest cobalt nanoclusters, **Co4/TiO₂** (7.0 nm) exhibited a typical continuous ASF distribution (with hydrocarbon chains up to C₇₀) with a single alpha value (0.87).

The evolution of the cobalt time yield (mol of CO converted per mol of total Co, per unit of time) of the catalysts during time is displayed in Figure 8a. Catalyst **Co1/TiO₂**, exhibited

a maximum in activity during the first hours of reaction (*ca.* 15 h⁻¹, after 3 h) and subsequently decreased to 10 h⁻¹ after 40 h of reaction. For the other catalysts, the initial maximum was not clearly observed and only exhibited a decrease in cobalt time yield when approaching the steady state. TEM analysis of the used catalysts (Supporting Information) demonstrated that the cobalt particle size did not change significantly, thus suggesting that cobalt sintering is not involved in the deactivation observed during the first hours of reaction. In Figure 8b, the catalyst activity and the surface specific activity (cobalt time yield and cobalt site yield) are presented as a function of the cobalt particle size. It is noteworthy that both the cobalt time yield and the cobalt site yield increased when the particle size decreased. The observed trend in activity for the series **Co1-4/TiO₂** could be correlated with the reducibility observed by TPR analysis, which increased as the cobalt particle size decreased. This trend contrasts with studies regarding the size effect of cobalt based catalysts in FTS in the sense that cobalt crystallites of only 1.6 nm are not only highly active but also stable under the tested reaction conditions.[32-36]

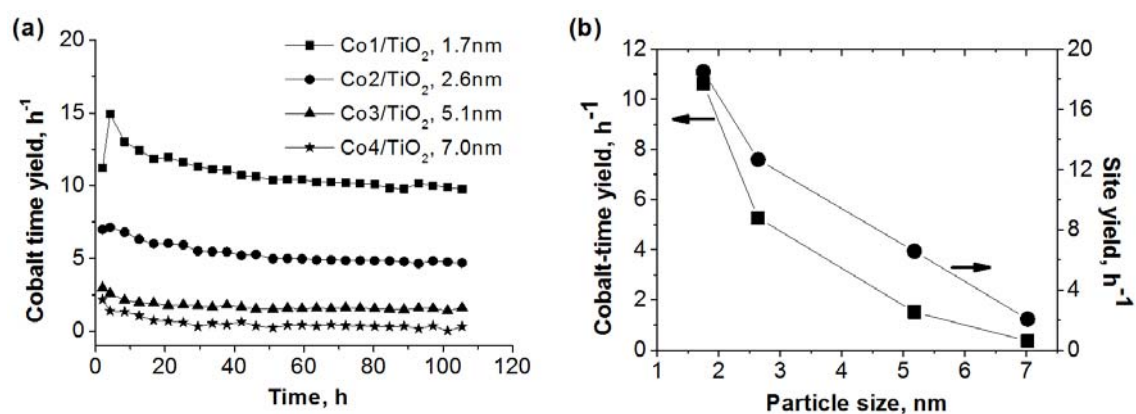


Figure 8. (a) Evolution of cobalt time yield in FT experiments. (b) Cobalt time and cobalt site yield after 46 h of reaction as function of the particle size of the CoNPs. Conditions: 7-10 wt% Co/TiO₂, 20 bar H₂/CO/N₂ (2:1:0.15), 5.62 ml/min, 240 °C.

Similar trends in activity were reported by Wang and co-workers who observed the superior performance in FT of ultra-small CoNPs supported on faujasite zeolite in comparison with larger NPs (CO conversion of 53 and 28 % for CoNPs of 1.7 and 29 nm, tested at 250 °C).[42] In this study, metallic CoNPs were prepared in the faujasite zeolite by the reduction of the Co²⁺-exchanged zeolite with NaBH₄ aqueous solutions. However, the authors did not give insights regarding the higher activity of the smaller CoNPs. Analysis of the product distribution suggested that the encapsulation of the CoNPs in the supercages of faujasite zeolite inhibited the formation of hydrocarbons with carbon numbers larger than 20 possibly because of the limit of the reaction space. In the present study, the observed decrease of the alpha value with the

decreasing size of the CoNPs could be attributed to the higher hydrogenation activity at the corners and edges, which are more important for those CoNPs of small size.

Regarding the unconventional stability of the relatively small CoNPs reported here in FTS, it is proposed that the boron contained in the CoNPs from the synthesis, could play the role of a stability promoter of the cobalt nanocrystallites.

Recently, boron was employed as a promoter to enhance the stability of Ni catalysts during steam reforming[46, 47] and cobalt based catalysts during Fischer-Tropsch synthesis.[41, 48] For instance, Saeys *et al.* used density functional theory (DFT) to study the effect of boron in cobalt catalysts and showed that boron atoms are thermodynamically stable at step and subsurface sites of a cobalt cluster under FT conditions.⁴⁶ The calculations hence suggested that boron promotion can selectively block the deposition, nucleation, and growth of resilient carbon species responsible for catalysts deactivation. The authors validated the theoretical calculations with catalytic tests, thus demonstrating that boron promotion reduced the deactivation rate in 6-fold, (for a 20 wt. % Co/ γ -Al₂O₃ catalysts containing 0.5 wt. % of boron) without affecting selectivity and activity.

Interestingly, elemental analysis of the colloidal NPs by XPS revealed that the Co/B atom ratio at the metal surface decreased from 2.2 to 0.8 as the cobalt particle size decreased from 7 to 1.7 nm. This observation suggests the enrichment of the metal surface by boron for the smaller CoNPs, which is in agreement with the observed decrease of the deactivation rate as the particle size of the CoNPs decreased from 7.0 to 2.6 nm (see Supporting Information).

As described above, these results provide evidence of the high catalytic activity of very small cobalt nanoparticles (1.7 nm) prepared by sodium borohydride in the Fischer–Tropsch synthesis. The unconventional stability in FTS of these small CoNPs is proposed to arise from the promoting effect of boron present into the catalyst structure.

4. Conclusions

A series of cobalt nanoparticles with sizes comprised between 1.7 and 7.0 nm were synthesized in water by chemical reduction with NaBH₄. This series of colloidal nanoparticles were easily immobilized on TiO₂ by simple impregnation method which did not require additional calcination treatments. This approach allowed the fine modulation of the particle size and permitted the detailed characterization of these cobalt nanoparticles before their immobilization on the solid support.

Structural analysis of the NPs indicated the amorphous structure of the NPs and revealed the presence of metallic cobalt, Co₂B and B(OH)₃ phases. Surface analysis indicated that the smaller the particle size, the higher the reduction degree of the nanoparticle is. Analysis of the TiO₂ supported catalysts showed that the particle size of the CoNPs and the trend in

reduction degree observed in the colloidal NPs remained unaltered after immobilisation while the reducibility of the catalysts increased with the decrease of the cobalt particle size.

Fischer-Tropsch experiments catalysed by the TiO₂ supported CoNPs revealed that the activity and surface specific activity increased when the cobalt particle size decreased from 7 to 1.7 nm. This trend in activity was correlated with the higher reducibility of the supported catalysts bearing smaller nanoparticles. The unconventional stability in FTS of these relatively small CoNPs was attributed to the promoting effect of boron on the stability of the cobalt nanocrystals.

5. Acknowledgements

The authors are grateful to Total S.A., the Spanish Ministerio de Economía y Competitividad (CTQ2013-43438-R and *Ramon y Cajal* fellowship to C. Godard) and the Generalitat de Catalunya (2014SGR670) for financial support. We also thank the Prof. Andrei Khodakov for his contribution concerning the experiments with supported catalysts.

References

- [1] V.R. Calderone, N.R. Shiju, D. Curulla-Ferré, S. Chambrey, A. Khodakov, A. Rose, J. Thiessen, A. Jess, G. Rothenberg, *Angew. Chem. Int. Ed.*, 52 (2013) 4397-4401.
- [2] A.Y. Khodakov, *Catal. Today*, 144 (2009) 251-257.
- [3] A. Steynberg, Fischer-Tropsch Technology. Studies in Surface Science and Catalysis, in: A. Steynberg, M. Dry (Eds.) Fischer-Tropsch Technology. Studies in Surface Science and Catalysis, Elsevier, 152, Amsterdam, The Netherlands, 2006, pp. 1-3.
- [4] L.P. Dancuart, A. Steynberg, Fischer-Tropsch based GTL technology: a new process?, in: B.H. Davis, M.L. Occelli (Eds.) Fischer-Tropsch synthesis, catalysts and catalysis, Elsevier, Eastbourne, UK, 2007, pp. 379-381.
- [5] Q. Zhang, J. Kang, Y. Wang, *ChemCatChem*, 2 (2010) 1030-1058.
- [6] J.H. Oh, J. Bae, S.J. Park, P.K. Khanna, K.W. Jun, *Catal. Lett.*, 130 (2009) 403-409.
- [7] A.Y. Khodakov, W. Chu, P. Fongarland, *Chem. Rev.*, 107 (2007) 1692-1744.
- [8] J. Zhang, J. Chen, Y. Ren, Y. Sun, *App. Catal. A-Gen*, 243 (2003) 121-133.
- [9] Y. Zhang, K. Hanayama, N. Tsubaki, *Catal. Commun.*, 7 (2006) 251-254.
- [10] K.P. de Jong, Deposition Precipitation Onto Pre-Shaped Carrier Bodies. Possibilities and Limitations, in: P.A.J.P.G. G. Poncelet, B. Delmon (Eds.) *Stud. Surf. Sci. Catal.*, Elsevier 1991, pp. 19-36.
- [11] C.M. Lok, Novel highly dispersed cobalt catalysts for improved Fischer-Tropsch productivity, in: B. Xinhe, X. Yide (Eds.) *Stud. Surf. Sci. Catal.*, Elsevier 2004, pp. 283-288.
- [12] A. Nakhaei Pour, M. Housaindokht, *Catal. Lett.*, 143 (2013) 1328-1338.
- [13] G. Prieto, A. Martínez, P. Concepción, R. Moreno-Tost, *J. Catal.*, 266 (2009) 129-144.
- [14] M. Trépanier, A.K. Dalai, N. Abatzoglou, *App. Catal. A-Gen*, 374 (2010) 79-86.
- [15] Y. Wang, H. Liu, Y. Jiang, *J. Chem. Soc., Chem. Commun.*, (1989) 1878-1879.
- [16] A. Roucoux, J. Schulz, H. Patin, *Chem. Rev.*, 102 (2002) 3757-3778.
- [17] X. Y. Quek, R. Pestman, R.A. van Santen, E.J.M. Hensen, *Catal. Sci. Technol.*, (2014).
- [18] V. Pendyala, W. Shafer, B. Davis, *Catal. Lett.*, 143 (2013) 895-901.
- [19] C. Wang, H. Zhao, H. Wang, L. Liu, C. Xiao, D. Ma, *Catal. Today*, 183 (2012) 143-153.
- [20] L. Liu, G. Sun, C. Wang, J. Yang, C. Xiao, H. Wang, D. Ma, Y. Kou, *Catal. Today*, 183 (2012) 136-142.
- [21] X.Y. Quek, Y. Guan, R.A. van Santen, E.J.M. Hensen, *ChemCatChem*, 3 (2011) 1735-1738.
- [22] C.X. Xiao, Z.P. Cai, T. Wang, Y. Kou, N. Yan, *Angew. Chem. Int. Ed.*, 47 (2008) 746-749.

- [23] A. Gual, J.A. Delgado, C. Godard, S. Castellón, D. Curulla-Ferré, C. Claver, *Top. Catal.*, 56 (2013) 1208-1219.
- [24] H. Wang, W. Zhou, J.X. Liu, R. Si, G. Sun, M.Q. Zhong, H.Y. Su, H.B. Zhao, J.A. Rodriguez, S.J. Pennycook, J.C. Idrobo, W.X. Li, Y. Kou, D. Ma, *J. Am. Chem. Soc.*, 135 (2013) 4149-4158.
- [25] H. Wang, Y. Kou, *Chin. J. Catal.*, 34 (2013) 1914-1925.
- [26] X.B. Fan, Z.Y. Tao, C.X. Xiao, F. Liu, Y. Kou, *Green Chem.*, 12 (2010) 795-797.
- [27] N. Yan, J.G. Zhang, Y. Tong, S. Yao, C. Xiao, Z. Li, Y. Kou, *Chem. Commun.*, (2009) 4423-4425.
- [28] X.B. Fan, N. Yan, Z.Y. Tao, D. Evans, C.X. Xiao, Y. Kou, *ChemSusChem*, 2 (2009) 941-943.
- [29] D.O. Silva, L. Luza, A. Gual, D.L. Baptista, F. Bernardi, M.J.M. Zapata, J. Morais, J. Dupont, *Nanoscale*, 6 (2014) 9085-9092.
- [30] D.O. Silva, J.D. Scholten, M.A. Gelesky, S.R. Teixeira, A.C.B. Dos Santos, E.F. Souza-Aguiar, J. Dupont, *ChemSusChem*, 1 (2008) 291-294.
- [31] M. Scariot, D.O. Silva, J.D. Scholten, G. Machado, S.R. Teixeira, M.A. Novak, G. Ebeling, J. Dupont, *Angew. Chem. Int. Ed.*, 47 (2008) 9075-9078.
- [32] G.L. Bezemer, J.H. Bitter, H.P.C.E. Kuipers, H. Oosterbeek, J.E. Holewijn, X. Xu, F. Kapteijn, A.J. van Dillen, K.P. de Jong, *J. Am. Chem. Soc.*, 128 (2006) 3956-3964.
- [33] J.Y. Park, Y.J. Lee, P.R. Karandikar, K.W. Jun, K.S. Ha, H.G. Park, *App. Catal. A-Gen*, 411-412 (2012) 15-23.
- [34] P.B. Radstake, J.P.d. Breejen, G.L. Bezemer, J.H. Bitter, K.P.d. Jong, V. Frøseth, A. Holmen, On the origin of the cobalt particle size effect in the fischer-tropsch synthesis, in: M.S. Fábio Bellot Noronha, S.-A. Eduardo Falabella (Eds.) *Stud. Surf. Sci. Catal.*, Elsevier2007, pp. 85-90.
- [35] J. van de Loosdrecht, B. Balzhinimaev, J.A. Dalmon, J.W. Niemantsverdriet, S.V. Tsybulya, A.M. Saib, P.J. van Berge, J.L. Visagie, *Catal. Today*, 123 (2007) 293-302.
- [36] E. van Steen, M. Claeys, M.E. Dry, J. van de Loosdrecht, E.L. Viljoen, J.L. Visagie, *J. Phys. Chem. B*, 109 (2005) 3575-3577.
- [37] E. Kikuchi, R. Sorita, H. Takahashi, T. Matsuda, *App. Catal. A-Gen*, 186 (1999) 121-128.
- [38] W. Xie, Y. Zhang, K. Liew, J. Li, *Sci. China Chem.*, 55 (2012) 1811-1818.
- [39] J.A. Delgado, S. Castellón, D. Curulla-Ferré, C. Claver, C. Godard, *Catal. Commun.*, 71 (2015) 88-92.
- [40] J.A. Delgado, C. Claver, S. Castellón, D. Curulla-Ferré, C. Godard, *ACS Catal.*, (2015) 4568-4578.
- [41] M. Saeys, K.F. Tan, J. Chang, A. Borgna, *Ind. Eng. Chem. Res.*, 49 (2010) 11098-11100.
- [42] Y. Wang, H. Wu, Q. Zhang, Q. Tang, *Micropor. Mesopor. Mat.*, 86 (2005) 38-49.
- [43] J. Garcia-Torres, E. Vallés, E. Gómez, *J. Nanopart. Res.*, 12 (2010) 2189-2199.
- [44] C. Petit, Z.L. Wang, M.P. Pileni, *J. Phys. Chem. B*, 109 (2005) 15309-15316.
- [45] G.N. Glavee, K.J. Klabunde, C.M. Sorensen, G.C. Hadjipanayis, *Langmuir*, 9 (1993) 162-169.
- [46] J. Xu, L. Chen, K.F. Tan, A. Borgna, M. Saeys, *J. Catal.*, 261 (2009) 158-165.
- [47] J. Xu, M. Saeys, *J. Catal.*, 242 (2006) 217-226.
- [48] K.F. Tan, J. Chang, A. Borgna, M. Saeys, *J. Catal.*, 280 (2011) 50-59.